Rapid Communications

Lifshitz transition and frustration of magnetic moments in infinite-layer NdNiO₂ upon hole doping

I. Leonov, ^{1,2} S. L. Skornyakov ^{1,2} and S. Y. Savrasov ³

¹M. N. Miheev Institute of Metal Physics, Russian Academy of Sciences, 620108 Yekaterinburg, Russia

²Ural Federal University, 620002 Yekaterinburg, Russia

³Department of Physics, University of California, Davis, California 95616, USA

(Received 12 March 2020; revised manuscript received 26 May 2020; accepted 27 May 2020; published 11 June 2020)

Motivated by the recent discovery of superconductivity in infinite-layer (Sr, Nd)NiO₂ films with Sr content $x \simeq 0.2$ [D. Li *et al.*, Nature (London) **572**, 624 (2019)], we examine the effects of electron correlations and Sr doping on the electronic structure, Fermi-surface topology, and magnetic correlations in (Nd, Sr)NiO₂ using a combination of dynamical mean-field theory of correlated electrons and band-structure methods. Our results reveal a remarkable orbital-selective renormalization of the Ni 3d bands, with $m^*/m \sim 3$ and 1.3 for the $d_{x^2-y^2}$ and $d_{3z^2-r^2}$ orbitals, respectively, that suggests orbital-dependent localization of the Ni 3d states. We find that upon hole doping, (Nd, Sr)NiO₂ undergoes a Lifshitz transition of the Fermi surface which is accompanied by a change of magnetic correlations from three-dimensional (3D) Néel *G*-type (111) to quasi-2D *C*-type (110). We show that magnetic interactions in (Nd, Sr)NiO₂ demonstrate an unanticipated frustration, which suppresses magnetic order, implying the importance of in-plane spin fluctuations to explain its superconductivity. Our results suggest that frustration is maximal for Sr doping $x \simeq 0.1$ –0.2, which is in agreement with an experimentally observed doping value Sr $x \simeq 0.2$ of superconducting (Nd, Sr)NiO₂.

DOI: 10.1103/PhysRevB.101.241108

The recent discovery of superconductivity in infinite-layer Sr-doped NdNiO₂ films (Nd_{0.8}Sr_{0.2}NiO₂) with a critical temperature up to $T_c \sim 15$ K has attracted a lot of attention from researchers around the world [1]. NdNiO₂ has a similar planar crystal structure to that of the parent "infinite-layer" superconductor CaCuO2, which exhibits superconductivity below $T_c \simeq 110$ K upon hole doping [2–4]. As Ni is isoelectronic to copper in NdNiO₂, it has a nominal d^9 configuration. Based on this, it was expected that, analogous to cuprates, the lowenergy physics of Sr-doped NdNiO₂ is dominated by electrons in the planar Ni $x^2 - y^2$ states. However, unlike cuprates, in the infinite-layer nickelate, the Ni $x^2 - y^2$ states are found to experience strong hybridization with the Nd 5d orbitals (primarily the $3z^2 - r^2$ and xy orbitals), yielding a noncuprate-like Fermi surface [5–7]. While the electronic structure of NdNiO₂ has recently been widely studied using various band-structure methods [8–11], model techniques [12–14], and density functional theory+dynamical mean-field theory (DFT + DMFT) [15,16] methods [17–22], the properties of Sr-doped NdNiO₂ are still poorly understood. For NdNiO₂, DFT + DMFT calculations reveal significant correlation effects within the Ni 3d orbitals, which are complicated by large hybridization with the Nd 5d states [17,21]. Moreover, based on the experiments two features that are central to copper oxides—the Zhang-Rice singlet and large planar spin fluctuations—were claimed to be absent (or diminished) in $(Nd, Sr)NiO_2$ [1,7].

Here, we explore the effects of electronic correlations and Sr doping on the electronic structure of (Nd, Sr)NiO₂ using a fully self-consistent in charge density DFT + DMFT method [15,16] implemented with plane-wave pseudopotentials [23,24]. We use this advanced computational method [25]

to study the Fermi-surface topology and magnetic correlations, as well as their impact on magnetism of $(Nd, Sr)NiO_2$ upon Sr doping.

We adopt the experimental lattice parameters measured for the Nd_{0.8}Sr_{0.2}NiO₂ film grown on the SrTiO₃ substrate (space group P4/mmm, lattice parameters a = 3.91 Å and c =3.37 Å) [1]. Following the literature, to avoid the numerical instabilities arising from the Nd 4f electrons, we focus on La^{3+} instead of the Nd^{3+} (4 f^3) ion [10,14,18]. (Hereafter, we assume La by saying Nd in our calculations). To explore the effect of Sr doping on the electronic structure of (Nd, Sr)NiO₂ we employ a rigid-band shift of the Fermi level within DFT. In our DFT + DMFT calculations we explicitly include the Ni 3d, Nd 5d, and O 2p valence states, by constructing a basis set of atomic-centered Wannier functions within the energy window spanned by these bands [26]. This allows us to take into account a charge transfer between the partially occupied Ni 3d, Nd 5d, and O 2p states [27], accompanied by the strong on-site Coulomb correlations of the Ni 3d electrons. We use the continuous-time hybridization expansion (segment) quantum Monte Carlo algorithm in order to solve the realistic many-body problem [28]. We take the average Hubbard U =6 eV, Hund's exchange J = 0.95 eV, and the fully localized double-counting correction as previously employed for rareearth nickelates RNiO₃ [29].

In Fig. 1 we display our results for the **k**-resolved spectra of paramagnetic (PM) (Nd, Sr)NiO₂ obtained by DFT + DMFT as a function of Sr doping x. Overall, our results agree well with those published previously [14,18,21]. For Sr x=0 we observe a band formed by the strongly mixed Ni and Nd $3z^2-r^2$ states crossing the Fermi level near the Γ point. Upon Sr x (hole) doping these states are seen to shift above the

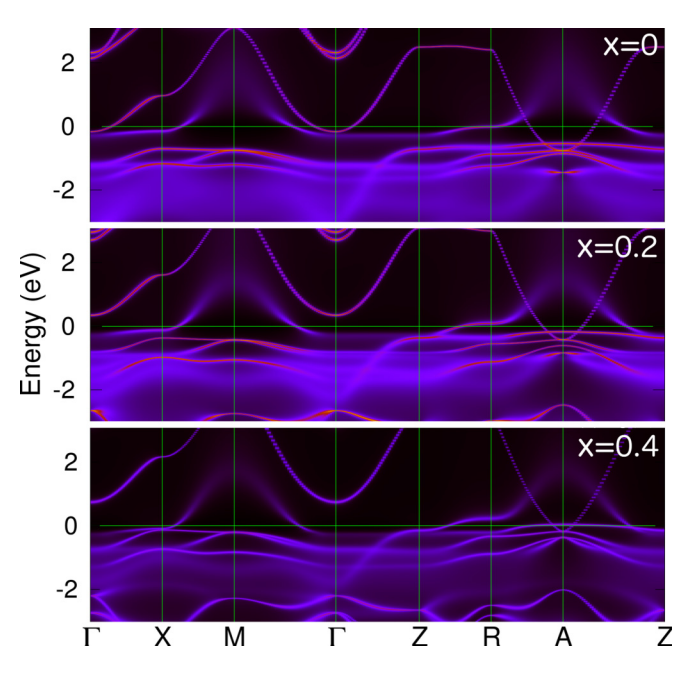


FIG. 1. **k**-resolved spectral function of PM (Nd, Sr)NiO₂ for Sr x = 0 (top), 0.2 (middle), and 0.4 (bottom) as obtained by DFT + DMFT at T = 290 K.

Fermi level, resulting in a change of the electronic structure of $(Nd, Sr)NiO_2$. It is accompanied by the disappearance of the electronlike states at the Γ and the formation of holelike structures near the Brillouin zone (BZ) R and A points. Our results therefore suggest a sign change of the Hall coefficient in $(Nd, Sr)NiO_2$ upon Sr doping, in agreement with recent experiments [30].

Our DFT + DMFT calculations reveal a remarkable orbital-selective renormalization of the partially occupied Ni $x^2 - y^2$ and $3z^2 - r^2$ bands (shown in Fig. 2). In particular, for Sr x = 0, the Ni $x^2 - y^2$ states exhibit a large mass

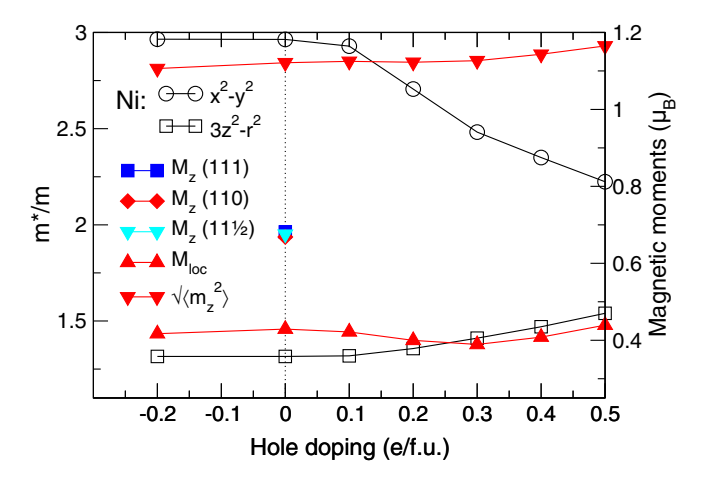


FIG. 2. Orbitally resolved quasiparticle mass enhancement m^*/m , instantaneous $\sqrt{\langle \hat{m}_z^2 \rangle}$, and fluctuating magnetic moments $M_{\rm loc} = \left[T \int_0^{1/T} \langle \hat{m}_z(\tau) \hat{m}_z(0) \rangle\right]^{1/2}$ of PM (Nd, Sr)NiO₂ calculated by DFT + DMFT at T=290 K. M_z : DFT + DMFT results for magnetization per Ni site for the Néel (111), C-type (110), and $(11\frac{1}{2})$ antiferromagnetic (AFM) states at T=290 K.

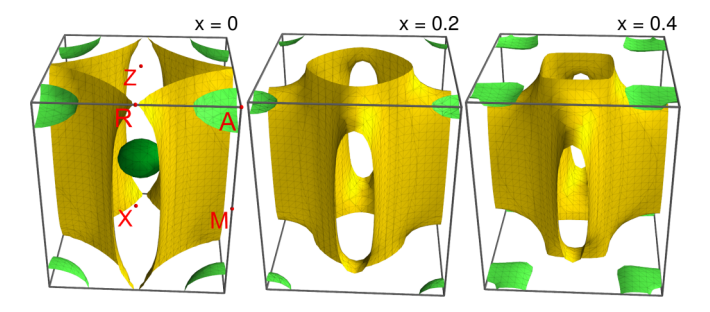


FIG. 3. Quasiparticle Fermi surface of PM (Nd, Sr)NiO₂ for Sr x = 0, 0.2, and 0.4 calculated by DFT + DMFT at T = 290 K. For clarity, different FS sheets are drawn in yellow, green, and dark green colors.

renormalization of $m^*/m \sim 3$, while correlation effects in the $3z^2 - r^2$ band are significantly weaker, $m^*/m \sim 1.3$. This behavior is consistent with sufficiently different occupations of the Ni $x^2 - y^2$ and $3z^2 - r^2$ orbitals. In fact, the $x^2 - y^2$ orbital occupancy for Sr x = 0 is close to half filling (~ 0.58 per spin orbit), while the $3z^2 - r^2$ orbitals are nearly fully occupied (~0.84). In addition, our analysis of the local spin susceptibility $\chi(\tau) = \langle \hat{m}_{\tau}(\tau) \hat{m}_{\tau}(0) \rangle$ (see Supplemental Material Fig. S1 [31]) suggests the proximity of the Ni $x^2 - y^2$ states to localization, while the Ni $3z^2 - r^2$ electrons are delocalized. Indeed, $\chi(\tau)$ for the Ni $3z^2 - r^2$ states is seen to decay fast to zero with the imaginary time τ , which is typical for itinerant behavior. In contrast to that, $\chi(\tau)$ for the $x^2 - y^2$ states is sufficiently larger, $\chi(0) = 0.72 \mu_{\rm B}^2$, slowly decaying to $\sim 0.07 \mu_{\rm B}^2$ at $\tau = \beta/2$. Our results therefore suggest that magnetic correlations in NdNiO₂ are at the verge of an orbitaldependent formation of local magnetic moments [17]. In agreement with this, the calculated (instantaneous) magnetic moment of Ni is about $\sqrt{\langle \hat{m}_z^2 \rangle} \simeq 1.1 \mu_B$, which is consistent with a nearly S = 1/2 state of nickel (see also Fig. S2 that shows orbitally resolved Ni 3d local moments).

Upon hole doping the Ni 3d occupations slightly decrease to 0.52 and 0.80 (per spin orbital) for the Ni $x^2 - y^2$ and $3z^2 - y^2$ r^2 orbitals, respectively, for Sr x = 0.5. This corresponds to a ~ 0.17 decrease of the total Wannier Ni 3d occupation, whereas the Nd 5d and O 2p state occupancies drop by \sim 0.21 and 0.06. In addition, we observe a gradual decrease of mass renormalization of the $x^2 - y^2$ states to $m^*/m \sim 2.3$ at Sr x = 0.5. In contrast to that for the $3z^2 - r^2$ orbital, m^*/m slightly increases to \sim 1.5. We notice no qualitative change in the self-energy upon changing of the Sr content x. The Ni 3d states obey a Fermi-liquid-like behavior with a weak damping at the Fermi energy. Moreover, doping with Sr does not affect much the magnetic moments in the paramagnetic phase of (Nd, Sr)NiO₂. Thus, the instantaneous magnetic moments $\sqrt{\langle \hat{m}_z^2 \rangle}$ tend to increase by only about 5%. Interestingly, in our model calculations (with absent self-consistency over the charge density, i.e., for the fixed tight-binding parameters of the DFT Wannier Hamiltonian) this increase is more significant, about 63%, suggesting the proximity to spin freezing, in accordance with recent model DMFT calculations [17].

Next, we calculate the quasiparticle Fermi surface (FS) of PM NdNiO₂ within DFT + DMFT. In Fig. 3 we show the dependence of the calculated FSs as a function of Sr x. We

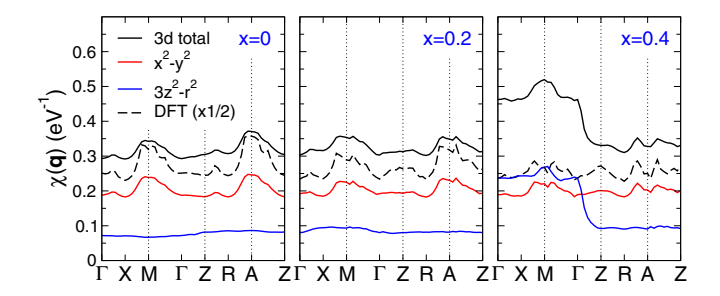


FIG. 4. Orbitally resolved static spin susceptibility $\chi(\mathbf{q})$ of (Nd, Sr)NiO₂ calculated by DFT + DMFT at T = 290 K.

note that our results for x = 0 are in qualitative agreement with previous band-structure studies [5,6,8,9]. In particular, we obtain that the FS consists of three FS sheets, with the elliptical FS centered at the BZ center (Γ point), originating from the mixed Ni 3d and Nd $3z^2 - r^2$ states. The electron FS pockets centered at the A point are mainly of the Ni xz/yz character. Similar to the cuprates, the FS of NdNiO₂ is dominated by the quasi-two-dimensional (quasi-2D) holelike FS sheet with a predominant Ni $x^2 - y^2$ character, centered at the A-M BZ edge. In close similarity to the cuprates, our results for the FS topology imply an in-plane nesting with magnetic vector $q_m = (110)$ (M point).

Upon an increase of the Sr content, we observe a remarkable change of the electronic structure of (Nd, Sr)NiO₂ which is associated with an entire reconstruction of the FS topology, i.e., a Lifshitz transition. Thus, at x=0.2 the elliptical FS centered at the Γ point vanishes. In addition, the holelike quasi-2D FS sheets at the top and the bottom of the BZ merge near the R point to a quasi-3D electron-like FS that forms a neck at the top and the bottom of the BZ. Overall, this suggests that the Lifshitz transition is accompanied by a reconstruction of magnetic correlations in infinite-layer (Nd, Sr)NiO₂ that appears near the experimentally observed doping Sr $x \simeq 0.2$.

We proceed with an analysis of the symmetry and strength of magnetic correlations in (Nd, Sr)NiO₂ and compute the momentum-dependent static magnetic susceptibility $\chi(\mathbf{q})$ within DFT + DMFT using the particle-hole bubble approximation. Orbital contributions of $\chi(\mathbf{q})$ along the BZ path and their dependence on Sr x are shown in Fig. 4. Our results for the total $\chi(\mathbf{q})$ as a function of Sr doping x are summarized in Fig. S3. Interestingly, for x = 0 our results for $\chi(\mathbf{q})$ exhibit two well-defined maxima at the M and A BZ points. This suggests the existence of (at least) two leading magnetic instabilities due to the Ni $x^2 - y^2$ states (for x = 0) with a wave vector near to $q_m = (110)$ and (111), that corresponds to the C-type and the Néel AFM ordering, respectively. In the same time $\chi(\mathbf{q})$ for the $3z^2 - r^2$ states is seen to be small and nearly q independent. We notice that $\chi(q)$ appears to be somewhat higher in the A than that in the M point. We therefore expect that the three-dimensional Néel AFM state is more energetically favorable than the quasi-2D C type (for Sr x = 0). In fact, this qualitative analysis agrees well with our total-energy calculations within the spin-polarized DFT and DFT + DMFT methods (see Fig. S4). Both reveal that for Sr x = 0 the Néel AFM ordering is more energetically favorable by about 3–4 meV/f.u. with respect to the C-type AFM and

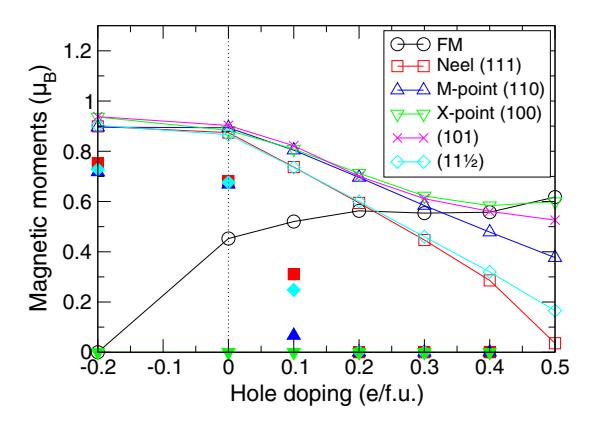


FIG. 5. Long-range ordered magnetic moments of Ni as a function of Sr x calculated for (Nd, Sr)NiO₂ by DFT (open symbols). DFT + DMFT results for the Néel, C-type (110), single stripe (100), and staggered dimer (11 $\frac{1}{2}$) AFM states at T=290 K are shown by solid symbols.

the PM state within DFT + DMFT, at T=290 K. We note that within DFT the Néel and the staggered dimer $(11\frac{1}{2})$ and C-type (110) states differ by about 5–7 meV/f.u., while the nonmagnetic state appears much above, by about 85 meV/f.u.

Our results for $\chi(\mathbf{q})$ and total energies suggest that various types of spin order are competing (nearly energetically degenerate) in (Nd, Sr)NiO₂. Indeed, for Sr x=0.2, $\chi(\mathbf{q})$ is seen to be nearly flat and degenerate at around the M and A points (see Fig. 4), implying possible frustration of the Ni 3d moments. Upon a further increase of Sr x, our results provide clear evidence of an entire reconstruction of magnetic correlations, with the $3z^2-r^2$ states now playing a major role, while for Sr x=0.4, $\chi(\mathbf{q})$ for the x^2-y^2 orbital is seen to be nearly flat (degenerate for different \mathbf{q}), suggesting in-plane frustration of the Ni 3d moments. The out-of-plane $3z^2-r^2$ orbital contribution reveals a flat maximum near the M point.

In Fig. 5 we show our results for the long-range ordered magnetic moments of nickel calculated within the spin-polarized DFT and DFT + DMFT. The latter are about $0.67\mu_{\rm B}/{\rm Ni}$ as obtained by DFT + DMFT for the Néel (111), C-type (110), and staggered dimer $(11\frac{1}{2})$ AFM states for Sr x=0, at T=290 K. Notably, we observe a sharp suppression of the calculated magnetization M_z and hence of the Néel temperature evaluated from the spin-polarized DFT + DMFT calculations with Sr x. In particular, for Sr x=0.2 we find no evidence of a magnetically ordered state at $T\geqslant 116$ K. Thus, all magnetic configurations discussed here, namely, the (100), (110), (111), and $(11\frac{1}{2})$ AFM and FM configurations, collapse in the PM state. That is, for Sr x=0.2, the Néel (Curie) temperature is much below the room temperature that suggests rising of quantum spin fluctuations with x.

We note, however, that an analysis of the finite-temperature DFT + DMFT results may often be problematic. For example, the single stripe (100) AFM and ferromagnetic orderings are found to be unstable at $T=290~\rm K$, i.e., both collapse to the PM state. We therefore first perform the spin-polarized DFT calculations of the ground-state energy differences between different magnetic states (see Fig. S4). In fact, the DFT calculations give qualitatively similar results to those obtained by DFT + DMFT with significantly larger values of

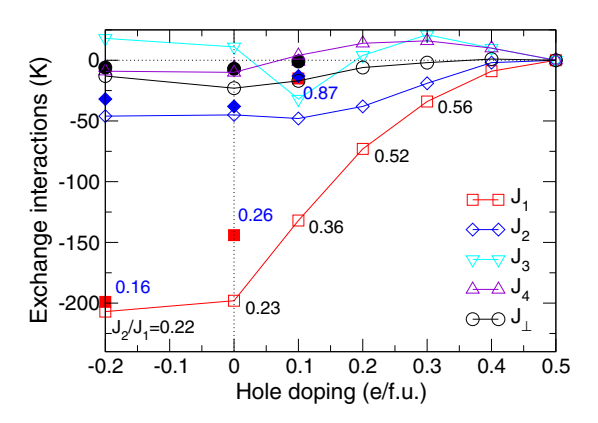


FIG. 6. Exchange interaction parameters [in-plane nearest-neighbor (NN) J_1 , next-nearest-neighbor J_2 , third NN J_3 , fourth NN J_4 , and interlayer coupling J_{\perp}] of Sr-doped NdNiO₂ calculated within spin-polarized DFT (open symbols) and DFT + DMFT (solid symbols).

the total energy difference (with respect to the nonmagnetic state) of $\sim 85 \text{ meV/f.u.}$, and 8 meV/f.u. for the C-type, Néel, and staggered dimer $(11\frac{1}{2})$, and single stripe (100) magnetic states, respectively. Both spin-polarized DFT and DFT + DMFT calculations reveal a near degeneracy of various types of spin orders, implying frustration of magnetic correlations in (Nd, Sr)NiO₂. The latter is most notable for a Sr content of about $x \simeq 0.2$ –0.3, which is close to the experimental Sr doping $x \simeq 0.2$. Moreover, the calculated magnetization for the various AFM states tends to decrease in both the DFT and DFT + DMFT calculations upon an increase of Sr x (see Fig. 5). In addition, within DFT + DMFT magnetization is found to sharply collapse to the PM state for Sr x > 0.1 at T = 290 K, suggesting a sharp increase of spin fluctuations with x.

Our results point out an anomalous sensitivity of the electronic structure and magnetic correlations of (Nd, Sr)NiO₂ with respect to the Sr x doping. In particular, we found a remarkable frustration of (orbital-dependent) magnetic moments of Ni sites near to the optimal Sr doping $x \simeq 0.2$. To help check these results, we computed magnetic exchange couplings within the spin-polarized DFT and DFT + DMFT using the magnetic force theorem [32]. Our findings for the Néel AFM state are summarized in Fig. 6. We observe that for Sr x = 0 the interlayer coupling is small and weakly antiferromagnetic, $J_{\perp} \sim -23$ K [33]. The in-plane couplings J_1 (nearest-neighbor) and J_2 (next-nearest-neighbor) are both antiferromagnetic and are sufficiently higher by modulus, ~ -198 and -45 K, respectively [34]. Most importantly, our results reveal a remarkable change of the J_2/J_1 ratio

with respect to Sr x, which is increasing from \sim 0.36 to 0.56 for x=0.1–0.3, i.e., near the experimental doping Sr $x\simeq 0.2$. While in DFT + DMFT magnetization is found to quickly collapse to the PM state for Sr x>0.1, the exchange couplings evaluated from the spin-polarized DFT + DMFT calculations do follow the same trend, with $J_2/J_1\simeq 0.26$ for Sr x=0, which is found to increase to 0.87 for Sr x=0.1.

Our findings resemble the behavior of a spin-1/2 frustrated J_1 - J_2 Heisenberg model on the 2D square lattice, with an unusual quantum spin-liquid ground state to appear in the highly frustrated region $J_2/J_1 \simeq 0.4$ –0.5, sandwiched between the Néel- and stripe-type (or valence-bond solid) ordered states [35]. This analogy is very striking, taking into account our results for the change of the electronic structure and magnetic coupling J_2/J_1 ratio in (Nd, Sr)NiO₂ with Sr x. Thus, the frustration region is sandwiched between the two different (longor short-range ordered) antiferromagnets [35]. We find that magnetic couplings in (Nd, Sr)NiO₂ near the optimal doping demonstrate an unanticipated frustration, which suppresses a long-range magnetic order (resulting in a drastic drop of the Néel temperature). Moreover, our results suggest that frustration is maximal for Sr doping x = 0.1-0.2 that corresponds to the highly frustrated region of the spin-1/2 frustrated J_1 - J_2 Heisenberg model. Overall, our results suggest the importance of in-plane spin fluctuations to explain superconductivity in (Nd, Sr)NiO₂, in contrast to previous claims [1]. We point out that the strong frustration of magnetic interactions in (Nd, Sr)NiO₂ suggests that superconductivity in infinite-layer (Nd, Sr)NiO₂ appears to be similar to that observed in iron chalcogenides and pnictides [36].

In conclusion, we show that upon hole doping $(Nd, Sr)NiO_2$ undergoes a Lifshitz transition of the Fermi surface which is accompanied by a reconstruction of magnetic correlations. Most importantly, magnetic interactions in $(Nd, Sr)NiO_2$ are found to demonstrate an unanticipated frustration. We find that frustration is maximal for Sr doping x=0.1-0.2 that nearly corresponds to the experimentally observed doping value of $(Nd, Sr)NiO_2$. Our results for $(Nd, Sr)NiO_2$ reveal a feature that is central to copper oxides as well as to iron chalcogenides and pnictides—large in-plane spin fluctuations. We propose that superconductivity in nickelates is strongly influenced, or even induced, by in-plane spin fluctuations.

We acknowledge support by the Russian Foundation for Basic Research (Project No. 18-32-20076). The theoretical analysis of the electronic structure was supported by the state assignment of Minobrnauki of Russia (theme "Electron" No. AAAA-A18-118020190098-5). S.Y.S. was supported by National Science Foundation DMR Grant No. 1832728.

^[1] D. Li, K. Lee, B. Y. Wang, M. Osada, S. Crossley *et al.*, Nature (London) **572**, 624 (2019).

^[2] M. Azuma, Z. Hiroi, M. Takano, Y. Bando, and Y. Takeda, Nature (London) 356, 775 (1992).

^[3] Y. Y. Peng, G. Dellea, M. Minola, M. Conni, A. Amorese *et al.*, Nat. Phys. 13, 1201 (2017).

^[4] S. Y. Savrasov and O. K. Andersen, Phys. Rev. Lett. 77, 4430 (1996).

^[5] V. I. Anisimov, D. Bukhvalov, and T. M. Rice, Phys. Rev. B 59, 7901 (1999); K.-W. Lee and W. E. Pickett, *ibid.* 70, 165109 (2004).

^[6] M.-Y. Choi, K.-W. Lee, and W. E. Pickett, Phys. Rev. B 101, 020503(R) (2020).

- [7] M. Hepting, D. Li, C. J. Jia, H. Lu, E. Paris *et al.*, Nat. Mater. 19, 381 (2020).
- [8] P. Jiang, L. Si, Z. Liao, and Z. Zhong, Phys. Rev. B 100, 201106(R) (2019); Y. Nomura, M. Hirayama, T. Tadano, Y. Yoshimoto, K. Nakamura, and R. Arita, *ibid.* 100, 205138 (2019); M. Jiang, M. Berciu, and G. A. Sawatzky, Phys. Rev. Lett. 124, 207004 (2020); J. Gao, Z. Wang, C. Fang, and H. Weng, arXiv:1909.04657; Z. Liu, Z. Ren, W. Zhu, Z. F. Wang, and J. Yang, npj Quantum Mater. 5, 31 (2020); E. Been, W.-S. Lee, H. Y. Hwang, Y. Cui, J. Zaanen *et al.*, arXiv:2002.12300; M.-Y. Choi, W. E. Pickett, and K.-W. Lee, arXiv:2005.03234.
- [9] H. Zhang, L. Jin, S. Wang, B. Xi, X. Shi, F. Ye, and J.-W. Mei, Phys. Rev. Research 2, 013214 (2020); Y. Fu, L. Wang, H. Cheng, S. Pei, X. Zhou et al., arXiv:1911.03177.
- [10] A. S. Botana and M. R. Norman, Phys. Rev. X 10, 011024 (2020)
- [11] B. Geisler and R. Pentcheva, arXiv:2001.03762.
- [12] G.-M. Zhang, Y.-F. Yang, and F.-C. Zhang, Phys. Rev. B 101, 020501(R) (2020)
- [13] X. Wu, D. Di Sante, T. Schwemmer, W. Hanke, H. Y. Hwang, S. Raghu, and R. Thomale, Phys. Rev. B 101, 060504(R) (2020).
- [14] H. Sakakibara, H. Usui, K. Suzuki, T. Kotani, H. Aoki, and K. Kuroki, arXiv:1909.00060.
- [15] A. Georges, G. Kotliar, W. Krauth, and M. J. Rozenberg, Rev. Mod. Phys. 68, 13 (1996); G. Kotliar, S. Y. Savrasov, K. Haule, V. S. Oudovenko, O. Parcollet, and C. A. Marianetti, *ibid.* 78, 865 (2006).
- [16] K. Haule, Phys. Rev. B 75, 155113 (2007); L. V. Pourovskii,
 B. Amadon, S. Biermann, and A. Georges, *ibid.* 76, 235101 (2007); B. Amadon, F. Lechermann, A. Georges, F. Jollet,
 T. O. Wehling, and A. I. Lichtenstein, *ibid.* 77, 205112 (2008);
 M. Aichhorn, L. Pourovskii, V. Vildosola, M. Ferrero, O. Parcollet, T. Miyake, A. Georges, and S. Biermann, *ibid.* 80, 085101 (2009); I. Leonov, L. Pourovskii, A. Georges, and I. A. Abrikosov, *ibid.* 94, 155135 (2016).
- [17] P. Werner and S. Hoshino, Phys. Rev. B 101, 041104(R) (2020).
- [18] S. Ryee, H. Yoon, T. J. Kim, M. Y. Jeong, and M. J. Han, Phys. Rev. B 101, 064513 (2020).
- [19] Y. Gu, S. Zhu, X. Wang, J. Hu, and H. Chen, Commun. Phys. 3, 84 (2020).
- [20] L. Si, W. Xiao, J. Kaufmann, J. M. Tomczak, Y. Lu, Z. Zhong, and K. Held, Phys. Rev. Lett. 124, 166402 (2020); M. Kitatani, L. Si, O. Janson, R. Arita, Z. Zhong, and K. Held, arXiv:2002.12230.
- [21] F. Lechermann, Phys. Rev. B 101, 081110(R) (2020).
- [22] J. Karp, A. S. Botana, M. R. Norman, H. Park, M. Zingl, and A. Millis, arXiv:2001.06441.
- [23] P. Giannozzi, S. Baroni, N. Bonini, M. Calandra, R. Car *et al.*, J. Phys.: Condens. Matter 21, 395502 (2009).
- [24] I. Leonov, N. Binggeli, D. Korotin, V. I. Anisimov, N. Stojić, and D. Vollhardt, Phys. Rev. Lett. 101, 096405 (2008); I. Leonov, D. Korotin, N. Binggeli, V. I. Anisimov, and D. Vollhardt, Phys. Rev. B 81, 075109 (2010).
- [25] Z. P. Yin, K. Haule, and G. Kotliar, Nat. Mater. 10, 932 (2011);
 7, 294 (2011); L. de' Medici, J. Mravlje, and A. Georges,
 Phys. Rev. Lett. 107, 256401 (2011); P. Werner, M. Casula,
 T. Miyake, F. Aryasetiawan, A. J. Millis, and S. Biermann,

- Nat. Phys. **8**, 331 (2012); I. Leonov, S. L. Skornyakov, V. I. Anisimov, and D. Vollhardt, Phys. Rev. Lett. **115**, 106402 (2015); S. L. Skornyakov, V. I. Anisimov, D. Vollhardt, and I. Leonov, Phys. Rev. B **96**, 035137 (2017); P. Villar Arribi and L. de'Medici, Phys. Rev. Lett. **121**, 197001 (2018); E. Greenberg, I. Leonov, S. Layek, Z. Konopkova, M. P. Pasternak, L. Dubrovinsky, R. Jeanloz, I. A. Abrikosov, and G. Kh. Rozenberg, Phys. Rev. X **8**, 031059 (2018); I. Leonov, G. K. Rozenberg, and I. A. Abrikosov, npj Comput. Mater. **5**, 90 (2019); X. Deng, K. M. Stadler, K. Haule, A. Weichselbaum, J. von Delft, and G. Kotliar, Nat. Commun. **10**, 2721 (2019).
- [26] N. Marzari, A. A. Mostofi, J. R. Yates, I. Souza, and D. Vanderbilt, Rev. Mod. Phys. 84, 1419 (2012); V. I. Anisimov, D. E. Kondakov, A. V. Kozhevnikov, I. A. Nekrasov, Z. V. Pchelkina *et al.*, Phys. Rev. B 71, 125119 (2005).
- [27] We note that the possible importance of the Nd 4f states has been pointed out in Refs. [6,12]. These studies, however, lead to different conclusions, suggesting Kondo-like (antiferro) and anti-Kondo (ferro) Nd 4f-5d exchange coupling, respectively.
- [28] E. Gull, A. J. Millis, A. I. Lichtenstein, A. N. Rubtsov, M. Troyer, and P. Werner, Rev. Mod. Phys. 83, 349 (2011).
- [29] H. Park, A. J. Millis, and C. A. Marianetti, Phys. Rev. B 89, 245133 (2014); E. A. Nowadnick, J. P. Ruf, H. Park, P. D. C. King, D. G. Schlom, K. M. Shen, and A. J. Millis, *ibid.* 92, 245109 (2015); I. Leonov, A. S. Belozerov, and S. L. Skornyakov, *ibid.* 100, 161112(R) (2019)
- [30] D. Li, B. Y. Wang, K. Lee, S. P. Harvey, M. Osada et al., arXiv:2003.08506.
- [31] See Supplemental Material at http://link.aps.org/supplemental/ 10.1103/PhysRevB.101.241108 for a detailed discussion of the electronic structure and magnetic properties of NdNiO₂ upon Sr doping.
- [32] A. I. Liechtenstein, M. I. Katsnelson, V. P. Antropov, and V. A. Gubanov, J. Magn. Magn. Mater. 67, 65 (1987); Y. O. Kvashnin, O. Grånäs, I. Di Marco, M. I. Katsnelson, A. I. Lichtenstein, and O. Eriksson, Phys. Rev. B 91, 125133 (2015).
- [33] Here, we adopt the following notation for the Heisenberg model, $H = -\sum_{i>j} J_{ij}e_ie_j$, where e_i are the unit vectors.
- [34] It is interesting to note that the experimental estimates give the antiferromagnetic exchange coupling $J \sim 25$ meV for NdNiO₂ written in the $H = J \sum_{ij} S_i S_j$, |S| = 1/2 notation of the Heisenberg model [9]. It is close to our estimate from the DFT total energy difference (in the same notation) of \sim 21 meV (or \sim 26 meV when $\langle S_i \rangle$ is replaced with the DFT magnetization per Ni site).
- [35] S.-S. Gong, W. Zhu, D. N. Sheng, O. I. Motrunich, and M. P. A. Fisher, Phys. Rev. Lett. 113, 027201 (2014); S. Morita, R. Kaneko, and M. Imada, J. Phys. Soc. Jpn. 84, 024720 (2015); L. Wang and A. W. Sandvik, Phys. Rev. Lett. 121, 107202 (2018).
- [36] Q. Si and E. Abrahams, Phys. Rev. Lett. 101, 076401 (2008); C. Fang, H. Yao, W.-F. Tsai, J. P. Hu, and S. A. Kivelson, Phys. Rev. B 77, 224509 (2008); C. Xu, M. Müller, and S. Sachdev, ibid. 78, 020501(R) (2008); M. J. Han, Q. Yin, W. E. Pickett, and S. Y. Savrasov, Phys. Rev. Lett. 102, 107003 (2009); J. K. Glasbrenner, I. I. Mazin, H. O. Jeschke, P. J. Hirschfeld, R. M. Fernandes, and R. Valentí, Nat. Phys. 11, 953 (2015); A. Baum, H. N. Ruiz, N. Lazarević, Y. Wang, T. Böhm et al., Commun. Phys. 2, 14 (2019).